

Simulation-based Vibration Sensor Placement for Centrifugal Pump Impeller Fault Detection

Alireza Zabihhesari^a, Farzad A. Shirazi^{b*}, Alireza Riasi^b, Mohammad Mahjoob^b, and Erfan Asnaashari^b

^a Department of Mechanical Engineering, York University, Ontario, Canada

^b School of Mechanical Engineering, College of Engineering, University of Tehran, Tehran, Iran

ARTICLE INFO

Article history:

Received: 24 February 2020

Accepted: 15 May 2020

Keywords:

Centrifugal Pump

Vibration

Fault Detection

Sensor Placement

Numerical Simulation

ABSTRACT

In this paper, a simulation-based method is proposed for optimal placement of vibration sensors for the purpose of fault detection in a centrifugal pump. The centrifugal pump was modeled to investigate the effect of vane tip fault on fluid flow patterns numerically. Pressure pulsations were investigated at different locations at the inner surface of the pump before and after the presence of the fault to determine the best location for installing vibration sensors on the pump casing. Experiments were also conducted by mounting accelerometers at various locations on the pump casing. Simulation and experimental results were then compared and a direct correlation between changes in PSD amplitudes of pressure and acceleration signals was observed. The optimum location for placement of an accelerometer was determined to be near the volute tongue on the casing where the highest level of pressure pulsations in the simulation was also calculated in the presence of vane tip fault.

1. Introduction

Vibration-based condition monitoring is one of the common techniques for fault detection in mechanical systems, which has widely been used over the past years [1-5]. The advantage of vibration sensors is their non-intrusive installation on the pump casing, if appropriate locations for positioning the accelerometers are found [6].

Several different methods of analyzing vibration signals have been investigated in the literature amongst which the frequency domain methods are popular. Orhan et al. [7] identified bearing faults in a centrifugal pump through analyzing measured vibration responses in the axial, horizontal and vertical directions in the frequency domain. In the recent two decades, the use of time-frequency domain methods such as wavelet transform in the fault detection of rotating machinery including turbomachinery has attracted many attentions as well [8].

The performance of artificial neural networks (ANNs) using appropriate features extracted from vibration signals has been investigated for fault detection in centrifugal pumps. Jami et al. [9] investigated the applicability of ANN for the detection and diagnosis of mechanical defects of impellers such as crack and imbalance. They used Statistical parameters, frequency peaks, and wavelet packet energy for data feature extraction, and a three-layer back-propagation ANN for fault recognition. Comparison of the network accuracy based on wavelet packet transform (WPT) features with time analysis and frequency analysis-based features, showed that WPT-ANN provides lower mean square errors, higher correlation coefficients and shorter training times.

Saberi et al. [10] proposed the Support Vector Machine (SVM), a method based on statistical learning theory (SLT), along with ANN for classifying the condition of a centrifugal pump. Six features including flow, temperature, suction pressure, discharge pressure, velocity, and vibration were used in their experiments. A comparison between SVM and ANN methods confirmed the superiority of SVM with some specific kernel functions.

Sakthivel et al. [11] applied ANN on features extracted from vibration signals to detect and classify bearing fault, impeller fault, seal fault and cavitation in a centrifugal pump. They investigated the performance of different dimensionality reduction techniques to increase the robustness of the classifier and to reduce the data processing load.

Nasiri et al. [12] analyzed vibration signals to detect cavitation in a centrifugal pump using ANN. Their model successfully identified three healthy/faulty conditions namely normal, moderate and fully developed cavitation. These automated fault detection methods can minimize human errors involved in interpreting measured vibration signals [13].

Impeller is a key component of a centrifugal pump that plays an important role in the performance of the pump. This component is always subject to various faults such as corrosion, erosion, wear, and vane tip damages. Al-Braik et al. [14] presented a model based on pressure pulsations. They first measured the vibrations of the outer surface of a pump by an accelerometer. Two pressure gauges were also installed at the inlet and outlet of the flow. The test was conducted in the healthy and 5 faulty vane tip conditions. The measurements were taken at 2900 rpm in 7 different flow rates. Their results demonstrated that frequencies more than 1 kHz which are dominant in the frequency spectrum (related to the flow

* Corresponding author. Tel.: +98-21-6111-4016; e-mail: fshirazi@ut.ac.ir

turbulence) do not change considerably with the presence of fault in the impeller. On the other hand, the presence of the fault changes additional frequencies generated by the interaction between the fluid flow, impeller and the surface of the pump. Therefore, it was concluded that the amplitude of the Blade Passing Frequency (BPF) and higher harmonics of the shaft rotational speed in the frequency spectrum are useful features in the diagnosis and classification of vane tip faults.

Processing of measured vibration signals from different components of a machine gives useful information that can be used in a damage detection process. Nevertheless, extracting appropriate features out of measured vibration signals and drawing a correct conclusion require a deep understanding of physical phenomena governing the system under investigation. Often, the accessibility to different operating mechanical components such as the impeller of turbomachines is extremely limited. Consequently, vibration signals related to these components are generally measured from bearings and outer surfaces that could contain misleading information. None of the mentioned works has proposed a systematic way on how to place accelerometers to obtain the richest data about the vibrating behavior of a pump. In addition, there is no record of the Computational Fluid Dynamics (CFD) simulations in the literature for sensor placement in fault detection applications.

For an effective Condition Monitoring (CM) a set of experimental data should be collected from the system in healthy and faulty situations and in different operating conditions. This procedure is costly and time-consuming. Recent developments of simulation software in the field of turbomachinery have enabled engineers to simulate the behavior of a machine in healthy and faulty conditions. Numerical simulations can give comprehensive information about the physics of the system under evaluation which are extremely useful especially for components with limited accessibility. Moreover, the training process of condition monitoring systems can be facilitated and is less time-consuming.

In addition to measuring vibration responses and analyzing them for the purpose of fault detection in centrifugal pumps, several studies have been conducted on the simulation of fluid flow in various pumps. Niazi et al. [15] used numerical simulations to estimate cavitation in a centrifugal pump. They compared simulation results with those obtained from experiments and concluded that numerical simulations can be used as appropriate tools for cavitation diagnosis at the design stage of the pump. Fatah et al. [16] used CFD and Finite Element (FE) models to investigate the dynamic performance of a centrifugal pump experiencing cavitation condition.

Pressure pulsations occur in centrifugal pumps due to various reasons that can adversely affect pump performance. These pulsations have been studied in centrifugal pumps using CFD. Although these studies were not done for the purpose of fault detection, reviewing them is beneficial to recognize the available simulation methods of fluid flow and interactions between impeller, volute and the inner surface of the pump.

Spence et al. [17] recorded the pressure pulsations obtained from a transient simulation at 15 different points in the volute and near the volute tongue with specific distances from the leading edge using the simulation software CFX-TASC flow. Simulation results were compared with the experimental ones to identify locations with maximum sensitivity to pressure pulsations. The impeller was modeled and meshed in CFX-Bladegen and CFX-Turbogrid, respectively. They presented a complete model of the fluid environment in a pump with two inlets and two volutes and

showed that the maximum sensitivity to pressure pulsations happens at the impeller outlet near the volute tongue. They also simulated all the possible boundary conditions for inlet and outlet of the pump. They demonstrated that the choice of boundary condition plays an important role in the rate of convergence in the transient analysis. The optimum conditions, considering the speed and accuracy of solution, obtained when mass flow at the inlet and static pressure at the outlet were set as boundary conditions.

Gonzalez et al. [18] investigated the interaction between the impeller and volute casing numerically. The simulation process was similar to that of [17] but the points for recording pressure pulsations were selected in a circular pattern, 10 degrees away from each other, around the impeller. Their results illustrated that pressure pulsations increase near the volute tongue. Furthermore, these pulsations were more sensible when the pump was operating away from its design point conditions.

Si et al. [19] simulated pressure pulsations using a combination of Reynolds-averaged Navier-Stokes equations, large Eddy and shear stress transport-Scale-Adaptive Simulations (SAS). They also conducted experimental tests by installing 8 pressure gauges on the middle plane of the volute. An increase in the intensity of pressure pulsations near the volute tongue was observed. BPF was the dominant frequency in the spectrum of pressure pulsations.

Barrio et al. [20] investigated the effect of four turbulence models: Spalart-Allmaras, $k - \epsilon$, $k - \omega$, and Reynolds Stress Model (RSM) on pump parameters such as head, flow rate and pressure variation amplitudes at BPF. They realized that changing the turbulence model has no effect on the head and flow rate of the pump, and changes in pressure variation amplitudes were less than 1%. However, it was found that $k - \epsilon$ model reduces the computation time considerably.

In this paper, a centrifugal pump is modeled in ANSYS CFX to investigate the effect of vane tip fault on fluid flow patterns through numerical simulations. Pressure pulsations are studied at different locations at the inner surface of the pump before and after the presence of the fault to determine the best location for installing vibration sensors on the pump casing. Experiments have also been conducted by mounting accelerometers at various locations on the pump. Simulation results are then compared with those obtained from experiments to match the observed trends in frequency response of measured signals. The rest of the paper is organized as follows. First, the experimental setup and the data acquisition system is explained. Then, the pump model in ANSYS CFX, and a thorough explanation of numerical simulation procedure of the centrifugal pump is presented. The time, and frequency domain analyses of pressure pulsation simulations, and vibration tests are discussed in the results section.

2. Experiment

2.1. Test Set-up

Experiments were carried out on a TecQuipment centrifugal pump test-rig (Model No. H302MK11) located in the Fluid Dynamics Lab in the School of Mechanical Engineering at the University of Tehran. The test-rig including a centrifugal pump and its electric motor is shown in Fig. 1. The data acquisition

2.3. Test Procedure

The objective of experiments was to collect vibration data from accelerometers at different positions on the casing of the centrifugal pump. The accelerometers were fixed on the casing by magnets (Fig. 3). The data was acquired when the pump was working around its nominal point of operation.



Figure 1. Centrifugal pump test-rig and the data acquisition system.

system used in the experiment will be explained in the next section.

Water flows from the bottom of the tank through a non-return valve and enters the pump after passing through a suction control valve. Water then moves into the volume measurement tank by passing through the discharge pipe. The volume measurement tank is used to calibrate the Venturi meter and to measure the volume of discharged water against time as well as the flow rate of the pump. Water finally enters the storage tank after moving through a hatch at the bottom of the volume measurement tank. As a result, the water travels through a closed hydraulic circuit having atmospheric pressure at both inlet and outlet (Fig. 2). A 2.2 kW (3 hp) DC motor was used to drive the centrifugal pump. The impeller is made of aluminum alloy 6061 and has 6 helical and backward-curved blades. The flow entry and exit angles are 15° and 67.5°, respectively.

The flow rate in all tests is measured using a Venturi flowmeter. The nominal mass flow rate of the pump at 2000 rpm is 3 kg/s,

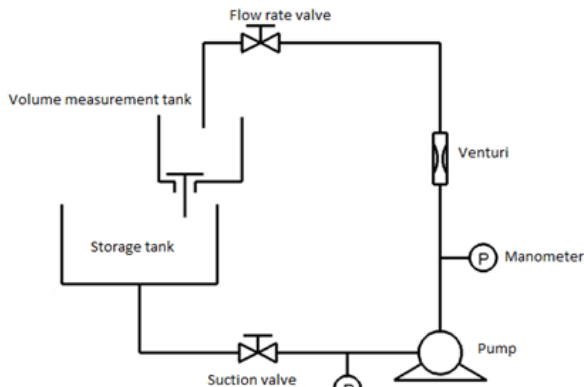


Figure 2. Hydraulic circuit of the experimental setup.

which can be altered to deviate from the operating point.

2.2. Data Acquisition

The data acquisition system includes a 6-channel data-logger (B&K 3560C, Denmark), 2 DJB A/120/VT piezoelectric accelerometers, an MM0024 laser tachometer, and PULSE LabShop Version 12.5.1 measurement software. Although it was expected that the damage in a blade tip mostly affects the BPF (equivalent to 200 Hz at 2000 rpm for this pump) and its second and third harmonics, the maximum sampling frequency of 25.6 kHz was initially chosen to ensure the accuracy of measurements. After taking a few readings, the power spectra of measured vibration responses revealed that the maximum frequency content is about 2 kHz. Therefore, a sampling frequency of 4096 Hz was finally assigned for all tests. The laser tachometer was utilized to measure the rotational speed of the pump and a manometer to measure the flow pressure.



Figure 3. Accelerometers installed on the pump casing.

Vane tip fault was introduced in the pump impeller with different sizes (2.5 mm, 5 mm and 7.5 mm) at the tip of a blade using a rasp. Fig. 4 illustrates the healthy and damaged impellers employed in this study.

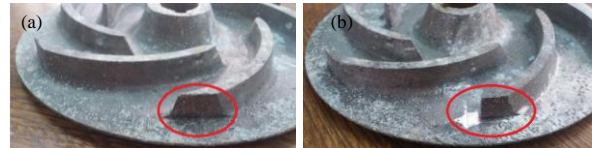


Figure 4. (a) Intact impeller, and (b) faulty impeller with 5 mm damage.

For each size of the fault, vibration data were recorded for 4s from different positions on the casing. Figure 5 shows a sample of vibration data obtained from the accelerometer installed at point B1 on the casing of the pump. Each test was repeated for 3 times and the averaged data was used to calculate the power spectra of signals.

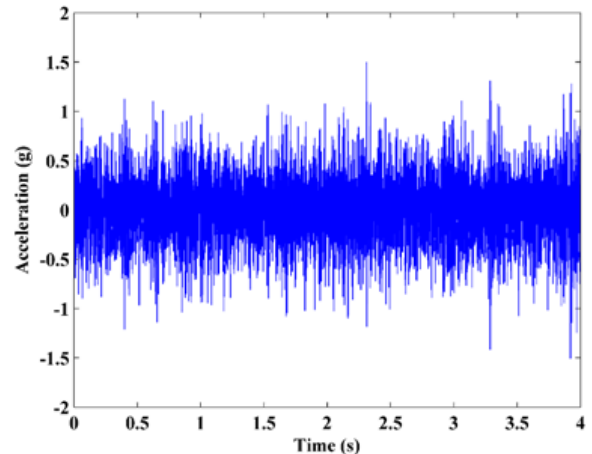


Figure 5. Measured accelerations from the sensor installed at point B1 on the pump casing.

3. Numerical Simulations

3.1. Geometric Modelling

In this study, the fluid flow in the centrifugal pump was modeled and analyzed within ANSYS CFX v17. The 3D models of the impeller and volute casing are shown in Fig. 6. Due to the complex geometry of the impeller and casing, we could not use the structured mesh. The unstructured grid provides higher flexibility and acceptable mesh quality for the automatic generation of mesh in complex geometries [21]. The unstructured hexahedral and tetrahedral elements have been used successfully in the literature for modeling centrifugal pumps [21-25]. Accordingly, tetrahedral and hexahedral elements were used in order to mesh different regions (Fig. 7). A localized refinement of mesh was employed at critical regions such as leading and trailing



Figure 6. 3D model of the impeller and volute.

edges of the impeller blades and the volute tongue. This is because the flow field properties variation such as pressure and velocity at these regions are expected to be substantial. The quality of generated mesh was inspected using three mesh parameters i.e. orthogonal quality (0.8532 ± 0.138 SD), skewness (0.2131 ± 0.109 SD), and aspect ratio (<13), which are found to be within appropriate ranges[21, 25].

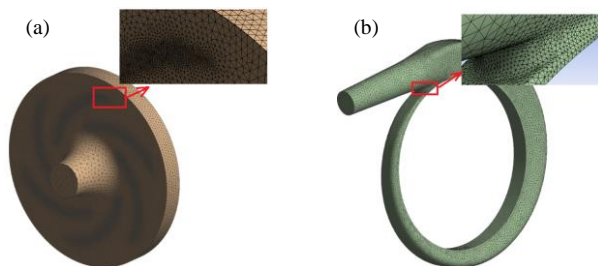


Figure 7. Generated mesh for the impeller (a) and the volute (b).

3.2. Turbulence Model Selection

The selection of appropriate turbulence model depends on the required accuracy of simulation results, available time, and computational resources. An appropriate model, especially in the transient state, is the one that considers the time required to obtain results in addition to the accuracy. $k - \epsilon$ model and scalable wall function are implemented in this study due to limited available computational resources, restriction on the mesh size of the boundary layer and trivial viscous effects in the viscous sublayer.

3.3. Boundary Conditions

Table 1 summarizes the various boundary conditions used at the inlet and the outlet of centrifugal pumps in the literature.

Considering the speed and accuracy of solution, the second choice in this table was found to be the optimum condition and used in this study.

Table 1. Boundary conditions at the inlet and outlet of the pump.

Location	1 st Condition	2 nd Condition	3 rd Condition
Pump inlet	Total pressure	Mass flow	Total pressure
Pump outlet	Mass flow	Static pressure	Static pressure

The CFD analysis involved two frames of reference, the rotational frame of reference and the stationary frame of reference. The impeller grids were set in the rotational frame of reference while the volute grids, inlet and outlet channels were set in the stationary frame of reference. The no-slip boundary condition was applied on the walls. The walls related to the surface of the impeller rotated at the speed of the impeller and those related to the casing were stationary. For steady-state analysis, the impeller-volute interaction was simulated using the Frozen Rotor model while the Transient Rotor Stator model was used for transient analysis.

In contrast to the volute of the pump that was fabricated by casting, the impeller was fabricated by CNC machining with lower surface roughness. Therefore, a higher value of surface roughness (0.05 mm) was considered for the volute compared to that of the impeller (0.02 mm).

Figure 8 shows the simulated fluid extracted from the geometric modeling of the centrifugal pump. The pump is divided into 4 sections including the inlet channel, impeller, volute and the outlet channel. The length of the inlet and outlet channels was considered long enough to avoid unwanted effects of boundary conditions on simulation results.

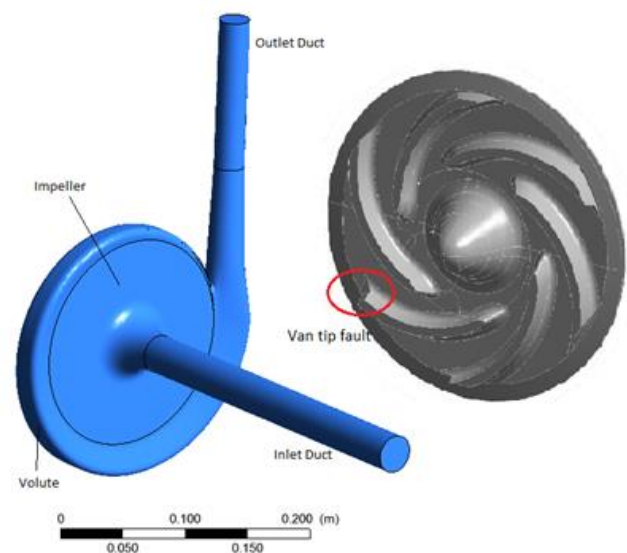


Figure 8. Environment of the simulated flow.

4. Results

4.1. Solution Verification

Mesh sensitivity analysis was performed to ensure that results were independent of the mesh size. For this purpose, the head and efficiency of the pump with intact impeller were considered. Figure 9 shows that increasing the number of elements from 2 to 2.7 million has insignificant effect on the head and efficiency values (less than 0.1%). Finally, 2,100,741 elements were found adequate to be used for meshing the pump in the healthy condition for a mesh independent simulation. Considering the small size of the created fault, the number of elements did not vary from healthy to faulty conditions.

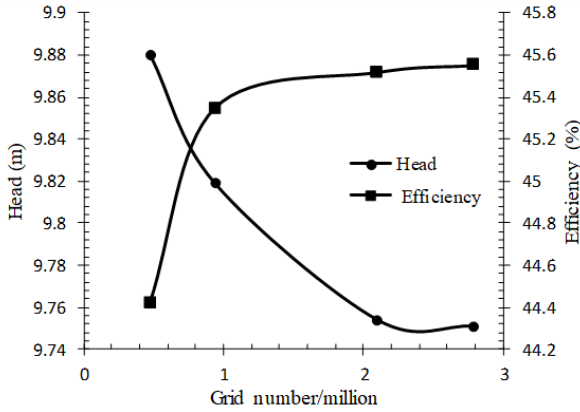


Figure 9. Mesh sensitivity of the solution.

4.2. Validation of Numerical Simulations

The validation process was carried out by making a comparison between the simulated results in the steady-state and those acquired from experiments. Figure 10 shows the variation of pump head against its flow rate in the healthy condition obtained from both simulations and experiments. An acceptable agreement can be observed between two results with a relative error of 0.15% at the design point (flow rate of 3 kg/s) and that of 2.8%, 1.0% and 7.6% at the flow rates of 3.6, 2.4 and 1.0 kg/s, respectively. The relative error increases when the pump was operated away from the optimum design point.

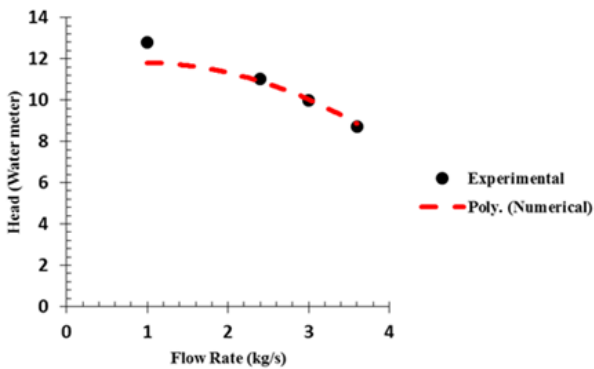


Figure 10. Comparison between simulated and experimental results in the healthy condition of the pump.

In the transient analysis, the time steps and total time are the most important parameters influencing the veracity of the simulation. The time step should be small enough to capture high-frequency variations during the simulation. Knowing that the BPF is the key parameter in this study, the time step was chosen such that frequencies higher than the BPF could also be considered. To this end, after running the simulation with several different time steps, the time step equivalent to one-degree rotation of the impeller (equals to 8.33×10^{-5} s at 2000 rpm) was selected. This resulted in dividing the time duration of the blade passing into 60

steps. Moreover, the residual convergence criterion for the continuity and Navier-Stokes equations was set at 10^{-5} .

4.3. Sensor Placement

The main objective of this study is to find optimum sensor locations on the centrifugal pump surface for the purpose of a specific fault detection. The fluid flow has different patterns in the points across the volute. Therefore, sensors need to be installed at locations where the effect of pressure pulsations is maximum, leading to an easier and time-efficient fault detection process. Previous studies have shown that bearing casing is the best location for mounting vibration sensors to identify mechanical faults such as unbalance, misalignment and bent shaft. This is sensible since mechanical forces are transferred to the foundation through bearings. In centrifugal pumps, however, mechanical and hydraulic faults could occur in different components of the pump such as impeller at the same time, making it impossible to differentiate the faults using bearing-only vibration measurements.

The vane tip fault, investigated in this study, exhibits the features of a mechanical and a hydraulic fault simultaneously. As a result, discovering the points where the greatest pressure pulsations happen is extremely useful in differentiating mechanical faults from hydraulic ones. Figure 11 shows a number of measurement points across the volute considered in simulations. In the experiments, sensors can only be placed on the outer surface of the volute. These points correspond to $A_1, B_1, C_1, D_1, E_1, F_1, G_1$ and H_1 .

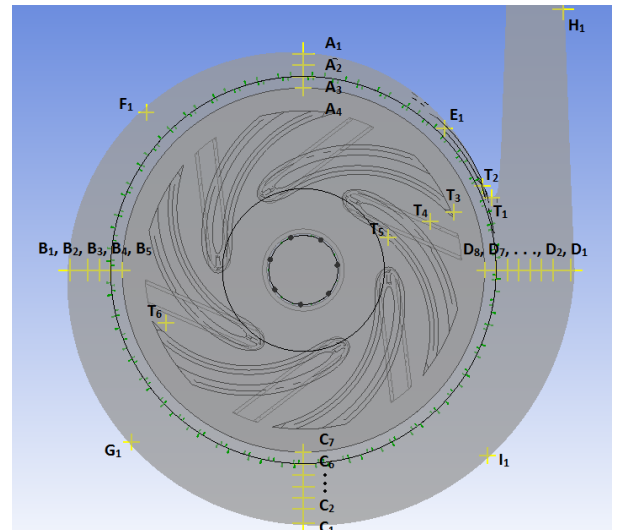


Figure 11. Selected locations for calculation of pressure pulsations in the numerical simulation.

4.4. Analysis of Time-domain Results

Since the focus of this study is on hydraulic effects of the vane tip fault, no mechanical faults are introduced in simulations. This

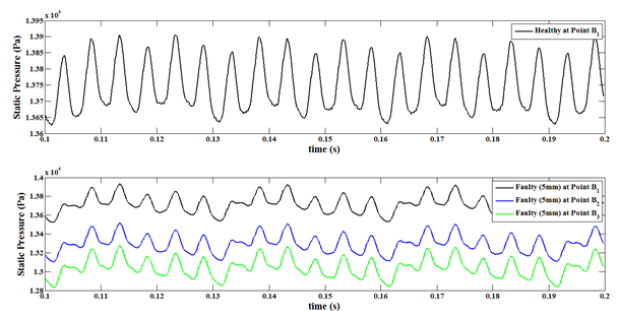


Figure 12. Trend of changes in pressure pulsations from point B_1 to B_3 .

means that simulation results will be purely due to changes in hydraulic conditions such as pressure pulsations.

The aim here is to know whether changes due to the presence of vane tip fault are strong enough to be detectable on the outer surface of the volute. To understand this, a number of reading points were selected along the distance between the vane tip and the outer surface of the volute (Fig. 11). Figure 12 shows the trend of changes in pressure pulsations from point B₁ to B₃ in presence of a 5mm vane tip loss. Similar patterns with different amplitudes can be seen in the pressure pulsations of these reading points. Moreover, the difference between the healthy and faulty conditions shows the significant effect of the vane tip fault on the pressure pulsations at all the points.

The volute of the pump is thick and stiff, and it can be assumed as a rigid body transferring the whole frequency content of pressure pulsations to its outer surface. This makes it possible to track changes in pressure pulsations through measuring the accelerations at the outer surface of the volute. Here, the purpose is to find a correlation between changes in frequency specifications of pressure and acceleration signals obtained from the simulation and experiment, respectively and use the correlation for future fault detection process.

Figures 13-15 compares the simulation results for different sizes of the fault at three distinct points of A₁, B₁ and E₁, where the difference between the healthy and faulty conditions becomes more distinguishable as the fault size grows.

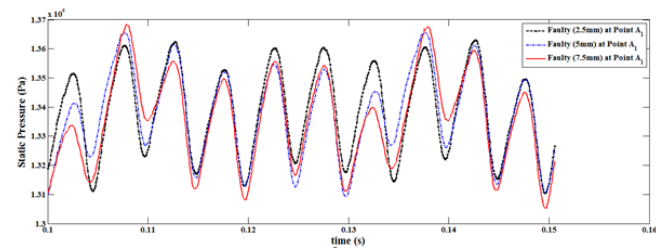


Figure 13. Pressure pulsations obtained from simulations at point A₁ in faulty conditions.

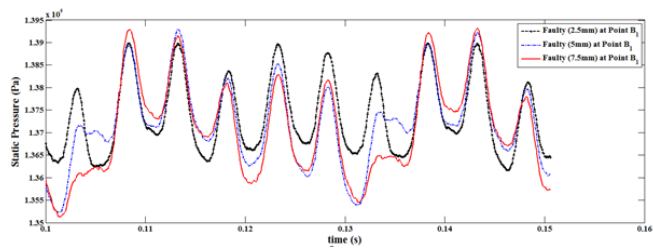


Figure 14. Pressure pulsations obtained from simulations at point B₁ in faulty conditions.

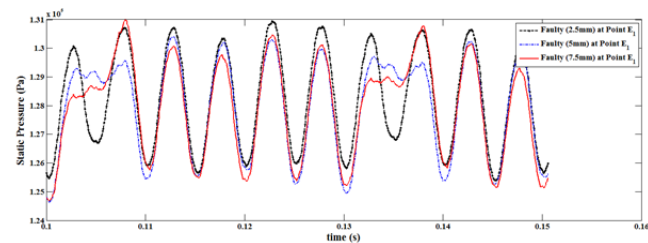


Figure 15. Pressure pulsations obtained from simulations at point E₁ in faulty conditions.

4.5. Analysis of Frequency-domain Results

In addition to the vane tip fault which has both mechanical and hydraulic effects in the system, there were some earlier unknown

faults in the pump making it difficult to extract the information related only to the vane tip. After analyzing the simulation results, it was determined that the vane tip fault has a significant effect on the pressure pulsations of the fluid in the volute. Therefore, pressure pulsations of the fluid are selected as a parameter to be investigated in vibration spectra.

4.5.1. Comparison of frequency spectra

As mentioned earlier, the focus of this study is to identify optimum locations on the volute for mounting sensors based on numerical simulations. Here, as shown in Fig. 16, the frequency spectra of pressure pulsations at different locations in the healthy condition of the volute are compared with each other.

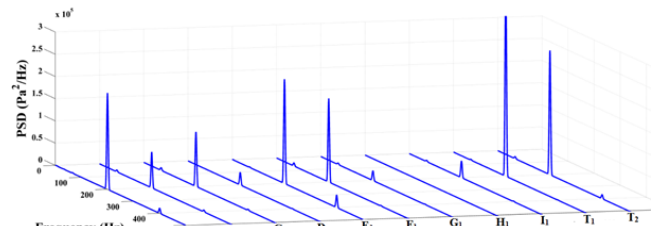


Figure 16. Power spectral density of pressure pulsations at different locations in the healthy condition, obtained from the numerical.

The dominant frequency in all of the spectra corresponds to the BPF, which equals to 200Hz at 2000RPM. Based on this observation as well as the previous studies from other researchers, the BPF is selected as one of the main features of pressure pulsations of the fluid. The desired locations are the ones with larger pressure pulsation amplitudes at the BPF, increasing the likelihood of picking those pulsations up using accelerometers mounted on the surface of the volute. According to Fig. 16, points A₁, E₁, T₁ and T₂, which are located near the volute tongue with minimum distance from the vane tip, have the largest amplitudes.

Experimental data have also been analyzed and the Power Spectral Densities (PSD) of vibration responses have been calculated (Fig. 17). PSD of signals provides an excellent measure to compare them in the frequency domain in the sense of power.

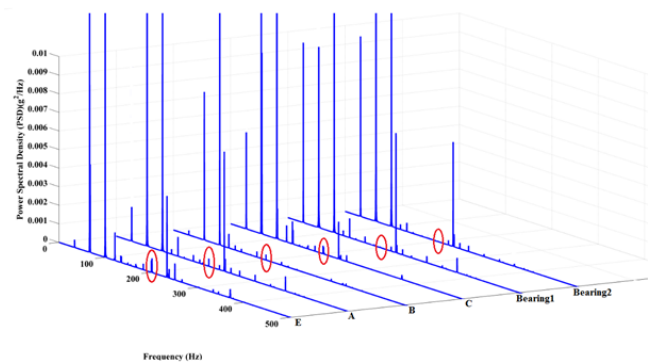


Figure 17. PSD of measured vibrations from the volute and bearings in the healthy condition.

Point E (equivalent of point E₁ in simulations) is the closest available location to the volute tongue for installing the accelerometer in experiments. Due to the shape of the volute, it was impossible to access points T₁ and T₂. Instead, accelerometers were mounted on the casing of the bearings. It should be noted that unlike the simulations, forces due to unbalance and other mechanical faults were present in the system in addition to forces of the fluid flow. As a result, the dominant frequencies in the spectra are related to the shaft rotational speed (33.33 Hz) and its second and third harmonics. In fact, the large amplitudes of the second and third harmonics (66.66 Hz and 100 Hz) in Fig. 17

shows the existence of probable faults such as misalignment and bent shaft in the system.

In Fig. 17, point E has the largest amplitude at the BPF. Moreover, at the bearings, the amplitude of the BPF is almost zero while the second and third harmonics of the rotational speed have their largest amplitudes compared to the other locations. This means that the bearing is not a suitable location for detecting the impeller-related faults, which particularly change pressure pulsations. Consequently, because of having a direct interaction with the fluid, the volute of the pump is the best place to mount the accelerometers in order to measure the changes in the BPF.

4.5.2. Vane tip fault in frequency spectra of pressure pulsations

The results of the numerical simulations have been used to investigate changes in the fluid flow after simulating the vane tip fault of sizes 2.5 mm, 5 mm and 7.5 mm in the impeller. The faulty impeller was meshed the same as when it is healthy. The simulation settings are identical for both the healthy and faulty conditions. Figures 18-20 demonstrate the PSD for the faulty impeller with different fault sizes at different locations. It can be observed that the simulated fault in one of the vanes of the impeller generates a few peaks at the rotating speed of the shaft (33.33 Hz), its second and third harmonics as well as the BPF.

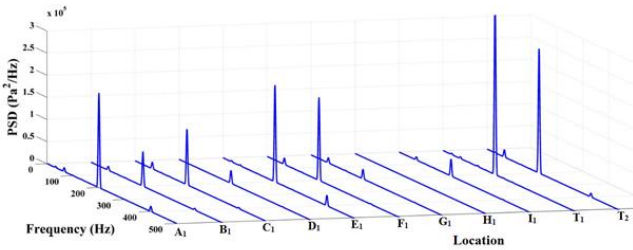


Figure 18. PSD for the faulty impeller with a damage size of 2.5 mm.

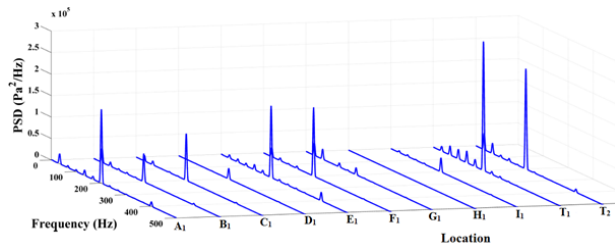


Figure 19. PSD for the faulty impeller with a damage size of 5 mm.

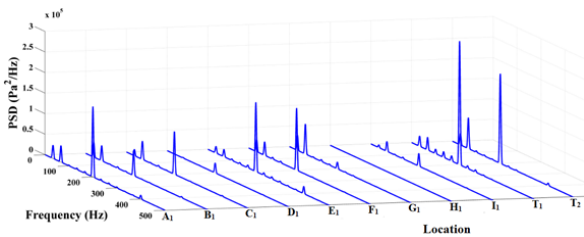


Figure 20. PSD for the faulty impeller with a damage size of 7.5 mm.

The amplitude of the harmonic peaks has a direct correlation with the size of the fault and becomes higher as the fault develops. On the contrary, the amplitude of the BPF at 200Hz has an inverse correlation with the fault size and becomes lower as the fault becomes larger. To give a clear image, the amplitudes of the PSD at the shaft speed and BPF for different locations are shown in Figs. 21 and 22. For the healthy impeller, the only significant

amplitude in the power spectrum of pressure pulsations corresponds to the BPF.

The simulation results revealed that the vane tip fault has a significant effect on the amplitude of the PSD of the pressure pulsations at the rotational speed of the shaft and BPF. Therefore, the amplitudes at 33.33 Hz and 200 Hz are advantageous features to be used in the vane fault detection process. This also needs to be tested experimentally through the analysis of measured acceleration data from the surface of the volute.

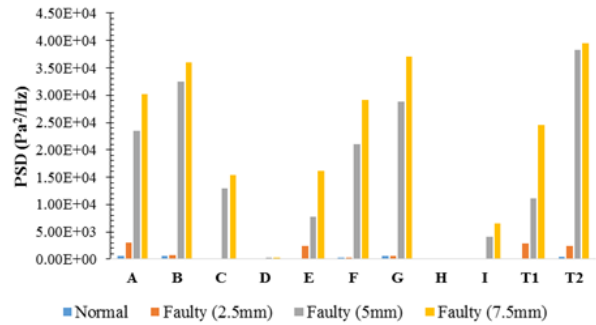


Figure 21. Amplitude of PSD of pressure pulsations at shaft rotational speed (33.33 Hz) obtained from numerical simulation.

4.5.3. Vane tip fault in frequency spectra of measured acceleration data

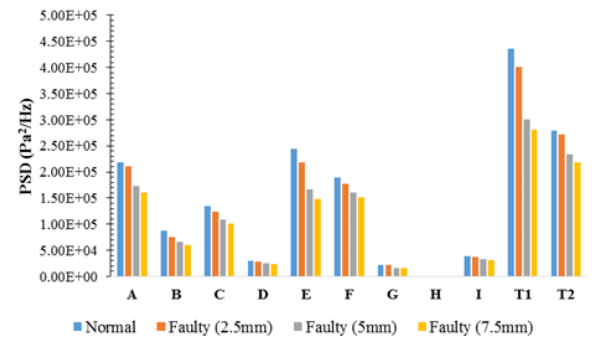


Figure 22. Amplitude of PSD of pressure pulsations at the BPF (200 Hz) obtained from numerical simulation.

measured acceleration data

Amplitudes of PSDs of the data in the rotational speed and its harmonics were calculated and analyzed. The experiments were conducted at the design (flow rate of 3 kg/s), and off-design (flow rates of 2.4 kg/s and 3.6 kg/s) points. Figures 23-26 display the amplitude of PSD at 1X and 6X frequencies for points A, B, C and E in the healthy and faulty conditions, respectively.

The analysis of the power spectra revealed that only the amplitudes at the first and sixth harmonics (related to the rotational speed and the BPF) show specific patterns. It was observed that the amplitude of the frequency spectrum at the second and third

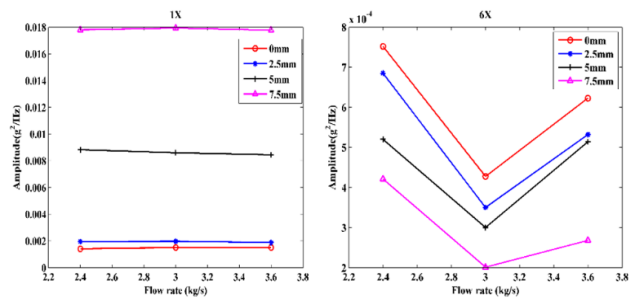


Figure 23. Amplitude of PSD in 1st and 6th harmonics of shaft speed at point A.

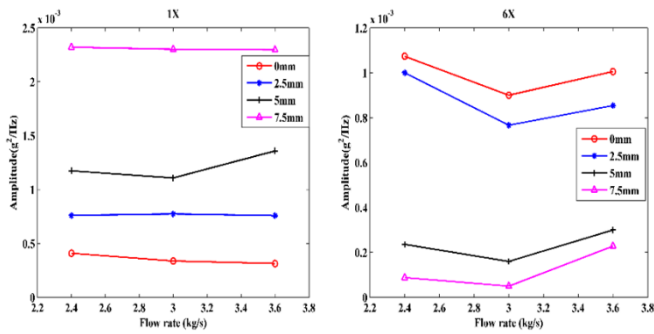


Figure 24. Amplitude of PSD in 1st and 6th harmonics of shaft speed at point B.

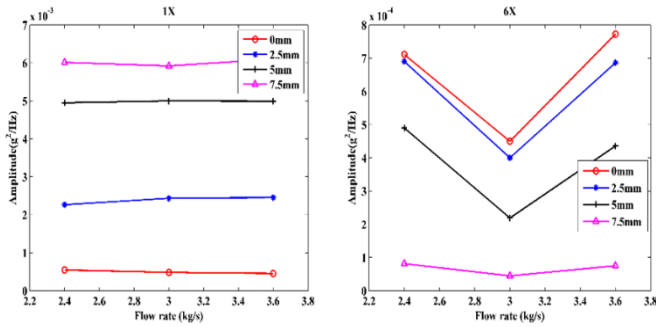


Figure 25. Amplitude of PSD in 1st and 6th harmonics of shaft speed at point C.

harmonics are larger than other harmonics, however, these amplitudes do not follow a specific pattern with the development of the fault. This is presumably due to the presence of other mechanical faults such as unbalance, misalignment or bent shaft in the pump. Moreover, the results of the numerical simulations have shown that the amplitude of frequency spectra at the rotational speed and its sixth harmonic (or the BPF) are the best parameters to differentiate the impeller faulty condition from the healthy state.

5. Conclusions

Figure 26. Amplitude of PSD in 1st and 6th harmonics of shaft speed at point E.

In this paper, a simulation-based method was proposed for the placement of vibration sensors to detect vane tip fault in a centrifugal pump. The centrifugal pump was modeled in ANSYS CFX to investigate the effect of vane tip fault on fluid flow through numerical simulations. Pressure pulsations were studied at different locations at the inner surface of the pump before and after the presence of the fault to determine the best location for the installation of vibration sensors on the pump casing. The difference between the healthy and faulty conditions showed the major effect of the vane tip fault on the pressure pulsations at all points. The optimum location for placement of an accelerometer was determined to be near the volute tongue where the highest level of pressure pulsations in the simulation was calculated in presence of vane tip fault. Experiments were also conducted by mounting accelerometers at various locations on the pump casing. Simulation and experimental results were then compared and a direct correlation between changes in PSD amplitudes of pressure and acceleration signals in 1X and 6X frequencies was observed. Therefore, the numerical simulation has provided an appropriate tool for investigating the effect of vane tip faults and can be used for generating different sets of data for future fault detection processes.

6. Acknowledgments

The authors would like to thank the Fluid Mechanics Lab at the University of Tehran for providing the opportunity of performing the experimental part of the work.

References

- [1] E. P. Carden, P. Fanning, Vibration based condition monitoring: a review, *Structural health monitoring*, Vol. 3, No. 4, pp. 355-377, 2004.
- [2] J. K. Sinha, K. Elbhah, A future possibility of vibration based condition monitoring of rotating machines, *Mechanical Systems and Signal Processing*, Vol. 34, No. 1-2, pp. 231-240, 2013.
- [3] A. Zabihi-Hesari, S. Ansari-Rad, F. A. Shirazi, M. Ayati, Fault detection and diagnosis of a 12-cylinder trainset diesel engine based on vibration signature analysis and neural network, *Proceedings of the Institution of Mechanical Engineers, Part C: Journal of Mechanical Engineering Science*, Vol. 233, No. 6, pp. 1910-1923, 2019.
- [4] F. A. Shirazi, M. Ayati, A. Zabihi-Hesari, S. Ansari-Rad, Fuel Injection Fault Detection in a Diesel Engine Based on Vibration Signature Analysis, in *Proceeding of, The 5th Iranian International NDT Conference*, pp. 1-7.
- [5] M. Ayati, F. A. Shirazi, S. Ansari-Rad, A. Zabihihesari, Classification-Based Fuel Injection Fault Detection of a Trainset Diesel Engine Using Vibration Signature Analysis, *Journal of Dynamic Systems, Measurement, and Control*, Vol. 142, No. 5, 2020.
- [6] R. Isermann, 2011, *Fault-diagnosis applications: model-based condition monitoring: actuators, drives, machinery, plants, sensors, and fault-tolerant systems*, Springer Science & Business Media.
- [7] S. Orhan, N. Aktürk, V. Celik, Vibration monitoring for defect diagnosis of rolling element bearings as a predictive maintenance tool: Comprehensive case studies, *Ndt & E International*, Vol. 39, No. 4, pp. 293-298, 2006.
- [8] Z. Peng, F. Chu, Application of the wavelet transform in machine condition monitoring and fault diagnostics: a review with bibliography, *Mechanical systems and signal processing*, Vol. 18, No. 2, pp. 199-221, 2004.
- [9] A. Jami, *Impeller fault detection under fluctuating flow conditions using artificial neural networks*, Thesis, University of Pretoria, 2016.
- [10] M. Saberi, A. Azadeh, A. Nourmohammadzadeh, P. Pazhoheshfar, Comparing performance and robustness of SVM and ANN for fault diagnosis in a centrifugal pump, in *Proceeding of*.
- [11] N. Sakhthivel, B. B. Nair, M. Elangovan, V. Sugumaran, S. Saravanmurugan, Comparison of dimensionality reduction techniques for the fault diagnosis of mono block centrifugal pump using vibration signals, *Engineering Science and Technology, an International Journal*, Vol. 17, No. 1, pp. 30-38, 2014.
- [12] M. Nasiri, M. Mahjoob, H. Vahid-Alizadeh, Vibration signature analysis for detecting cavitation in centrifugal pumps using neural networks, in *Proceeding of, IEEE*, pp. 632-635.
- [13] M. A. S. Al Tobi, G. Bevan, K. Ramachandran, P. Wallace, D. Harrison, Experimental set-up for investigation of fault diagnosis of a centrifugal pump, *Int. J. Mech. Aerospace Ind. Mechatronic Manuf. Eng.*, Vol. 11, No. 3, pp. 481-485, 2017.
- [14] A. Al-Braik, O. Hamomd, F. Gu, A. Ball, Diagnosis of impeller faults in a centrifugal pump based on spectrum analysis of vibration signals, in *Proceeding of, British Institute of Non-Destructive Testing*, pp.
- [15] E. Niazi, M. Mahjoob, A. Bangian, Experimental and numerical study of cavitation in centrifugal pumps, in

Proceeding of, American Society of Mechanical Engineers Digital Collection, pp. 395-400.

- [16] A. A. Abdel Fatah, M. A. Hassan, M. Lotfy, A. S. Dimitri, Health Monitoring of Centrifugal Pumps Using Digital Models, *Journal of Dynamic Systems, Measurement, and Control*, Vol. 141, No. 9, 2019.
- [17] R. Spence, J. Amaral-Teixeira, Investigation into pressure pulsations in a centrifugal pump using numerical methods supported by industrial tests, *Computers & fluids*, Vol. 37, No. 6, pp. 690-704, 2008.
- [18] J. Gonzá'lez, J. n. Ferná'ndez, E. Blanco, C. Santolaria, Numerical simulation of the dynamic effects due to impeller-volute interaction in a centrifugal pump, *J. Fluids Eng.*, Vol. 124, No. 2, pp. 348-355, 2002.
- [19] C. Mullen, T. Vaughan, M. Voisin, M. Brennan, P. Layrolle, L. McNamara, Cell morphology and focal adhesion location alters internal cell stress, *Journal of The Royal Society Interface*, Vol. 11, No. 101, pp. 20140885, 2014.
- [20] R. Barrio, J. Parrondo, E. Blanco, Numerical analysis of the unsteady flow in the near-tongue region in a volute-type centrifugal pump for different operating points, *Computers & Fluids*, Vol. 39, No. 5, pp. 859-870, 2010.
- [21] A. A. Noon, M.-H. Kim, Erosion wear on centrifugal pump casing due to slurry flow, *Wear*, Vol. 364, pp. 103-111, 2016.
- [22] K. Guleren, A. Pinarbasi, Numerical simulation of the stalled flow within a vaned centrifugal pump, *Proceedings of the Institution of Mechanical Engineers, Part C: Journal of Mechanical Engineering Science*, Vol. 218, No. 4, pp. 425-435, 2004.
- [23] Y. Fu, J. Yuan, S. Yuan, G. Pace, L. d'Agostino, P. Huang, X. Li, Numerical and experimental analysis of flow phenomena in a centrifugal pump operating under low flow rates, *Journal of Fluids Engineering*, Vol. 137, No. 1, 2015.
- [24] K. Cheah, T. Lee, S. Winoto, Z. Zhao, Numerical flow simulation in a centrifugal pump at design and off-design conditions, *International Journal of Rotating Machinery*, Vol. 2007, 2007.
- [25] L. Obregon, G. Valencia, J. D. Forero, Efficiency Optimization Study of a Centrifugal Pump for Industrial Dredging Applications Using CFD, 2019.